

ChemComm

Accepted Manuscript

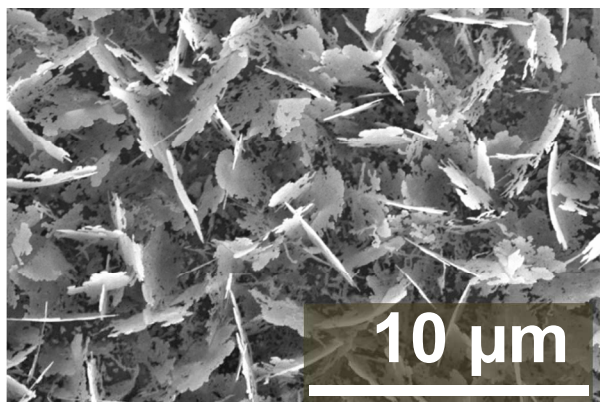


This is an *Accepted Manuscript*, which has been through the Royal Society of Chemistry peer review process and has been accepted for publication.

Accepted Manuscripts are published online shortly after acceptance, before technical editing, formatting and proof reading. Using this free service, authors can make their results available to the community, in citable form, before we publish the edited article. We will replace this *Accepted Manuscript* with the edited and formatted *Advance Article* as soon as it is available.

You can find more information about *Accepted Manuscripts* in the [Information for Authors](#).

Please note that technical editing may introduce minor changes to the text and/or graphics, which may alter content. The journal's standard [Terms & Conditions](#) and the [Ethical guidelines](#) still apply. In no event shall the Royal Society of Chemistry be held responsible for any errors or omissions in this *Accepted Manuscript* or any consequences arising from the use of any information it contains.



CZTS nanoplatelets have been grown using spray pyrolysis of a mixture of copper-, zinc- and tin-diethyldithiocarbamate as precursors.

COMMUNICATION

Spray pyrolysis of CZTS nanoplatelets

Cite this: DOI: 10.1039/x0xx00000x

S.Exarhos^a, K.N.Bozhilov^{b,c}, L.Mangolini^{a,c}Received 00th January 2012,
Accepted 00th January 2012

DOI: 10.1039/x0xx00000x

www.rsc.org/

We demonstrate that copper-zinc-tin-sulphide nanoplatelets can be directly grown onto a molybdenum-coated substrate using spray pyrolysis starting from a mixture of metal thiocarbamates precursors. The structure and phase purity of the nanoplatelets is discussed in details.

Copper-zinc-tin-sulphide (CZTS) has emerged as a potential low-cost, earth-abundant material for photovoltaic (PV) applications¹⁻⁴. The abundance of its constituents is a clear advantage compared to other materials for thin film PV application, such as cadmium telluride (CdTe) or copper-indium-gallium-sulphide (CIGS). While state-of-the-art devices based on CZTS absorber layers have achieved a power conversion exceeding 12%⁵, this value is significantly lower than the ~30% maximum theoretical (Shockley Queisser⁶) efficiency for this material. An improved understanding of its properties, including their dependence on the synthesis approach, is needed to make this material feasible for commercial applications. Our contribution focuses on the direct growth of CZTS layers onto molybdenum-coated soda-lime glass via spray pyrolysis. The direct growth of CZTS thin films using this simple and scalable technique would be highly desirable. There are only few reports on the production of CZTS films using spray pyrolysis⁷⁻¹⁰, and are all based on nebulizing a solution containing metal salts (chlorides and acetates) and using thiourea as sulphur source. In these reports, the precursors chemically react to form the desired film and the by-products are volatile (chemical spray pyrolysis). We have instead used metal thiocarbamates as precursors. These precursors thermally decompose into their corresponding metal sulphides upon heating to temperatures in the 170°C-250°C range^{11, 12}. Zinc diethyldithiocarbamate has been used for the production of zinc sulphide nanoparticles via aerosol spray pyrolysis¹³. Our group has shown that a similar technique can produce copper sulphide nanoparticles starting from copper diethyldithiocarbamate¹⁴. In this work, copper, zinc and tin diethyldithiocarbamates [Cu(dedc)₂, Zn(dedc)₂ and Sn(dedc)₄ respectively] are prepared following the recipe described by Khare et al.¹². To briefly summarize, the metal chloride precursors are reacted with sodium diethyldithiocarbamate in an ethanol solution. The precipitate is then purified by filtering

and rinsing multiple times with large amounts of water and ethanol. After vacuum drying, the copper, zinc and tin diethyldithiocarbamates are dissolved in toluene in a 2:1:1 molar ratio with a typical total concentration of 10 mg/ml. The solution is aerosolized using a one-nozzle collision nebulizer from BGI, Inc. Typically, 50 ml of solution are nebulized for each coating run. Argon as gas carrier is flown at a rate of 0.5 standard cubic feet per hour (SCFH). Under these conditions the nebulization rate is 2 ml per minute, and each coating run lasts approximately 30 minutes. The aerosol is aerodynamically dragged through an orifice with a diameter of 1/8". The flow expands into a 2" quartz tube placed in a temperature controlled tube furnace. A 1" diameter substrate holder is placed inside the tube furnace at a distance of 12" from the orifice. A rotary vane vacuum pump is used to maintain a pressure of 20 kPa downstream of the orifice. Growth occurs in a sealed and oxygen-free environment. Under vacuum, the system leakage rate is <5 milli Torr/minute. The system is purged with argon before growth begins. A thermocouple is inserted into the substrate holder to get a more precise reading of the growth temperature. Typically the substrate temperature during the film growth is 20°C below the tube

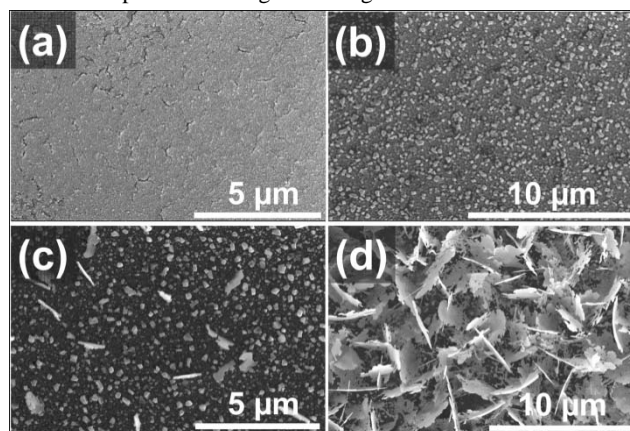


Figure 1. SEM micrographs of samples grown on molybdenum-coated soda lime glass at the following temperatures: (a) 360°C, (b) 400°C, (c) 440°C and (d) 460°C.

furnace temperature set point. Molybdenum-coated soda lime glass is used as substrate. A schematic of the experimental apparatus is shown in the Supplementary Information. Figure 1 shows top-down scanning electron microscopy (SEM) images of films grown at increasing tube furnace temperatures. This analysis was performed using a FEI NNS450-FEG SEM. The temperatures reported in the figure refer to the tube furnace temperature, which as mentioned above is 20°C higher than the actual substrate temperature. For consistency we will refer to the tube furnace temperature for the rest of the manuscript.

Films grown at 360°C are relatively smooth and uniform. Cross sectional SEM indicates that at the lowest temperature the film thickness is below 100 nm, indicative of a low growth rate. At 400°C the film is less uniform and composed of particles. At 440°C anisotropic growth is noticeable. At 460°C, the substrate is covered by a dense array of platelets with an average height of ~5 μm. Raman, shown in figure 2, is consistent with the spectra reported in the literature for CZTS structures^{15, 16}. The Raman spectrum for the sample grown at the lowest temperature does not have well defined features except for a peak at 408 cm⁻¹ which we attribute to MoS₂¹⁷, likely the result of the sulfurization of the substrate during film growth. The MoS₂ signal is clearly detectable because of the low thickness of this film. At 400°C the film presents a well-distinguishable peak at 338 cm⁻¹, characteristic of CZTS, and a weak signal at ~408 cm⁻¹. The MoS₂ signal is even smaller in the Raman for the sample grown at 440°C, and absent for the sample grown at 460°C. The three samples grown at higher temperature have clear peaks at 288 cm⁻¹, 338 cm⁻¹ and 380 cm⁻¹, in excellent agreement with the values reported for CZTS^{15, 16}.

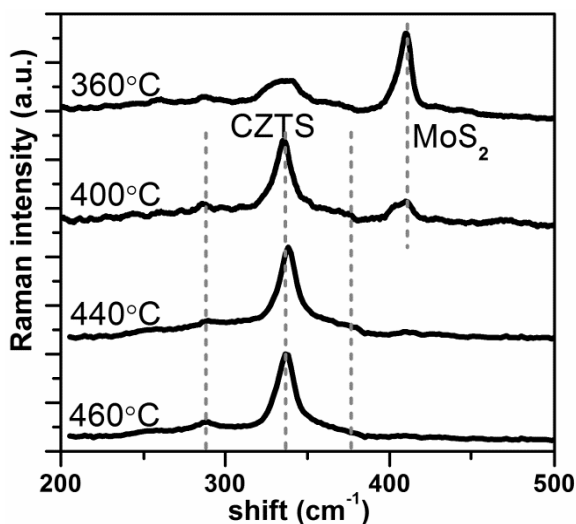


Figure 2. Raman spectra as a function of growth temperature.

XRD and optical characterization, shown in figure 3, also confirm the successful synthesis of CZTS. Figure 3a shows the XRD spectrum for the sample grown at 460°C (see figure 1d). The peak position is in excellent agreement with other XRD measurements reported in the literature^{2, 4, 15, 16}. The peak at 40.6° is from the Mo-coated substrate. The clearly distinguishable peaks at 18.3°, 28.5°, 33°, 47.3°, 56.1° and 58.9° can be assigned to 101, 112, 200, 204, 312 and 224 reflections of the tetragonal CZST, respectively. With the exception of the sample grown at the lowest temperature, whose XRD spectrum is quite noisy due to its small thickness and probably poor crystallinity, all other samples have XRD spectra similar to the one shown in figure 3a. As discussed by Cheng et al.¹⁵, this does not rule out that other phases may be present in the films grown using the spray pyrolysis technique, since zinc sulphide (ZnS) and copper-

tin-sulphide (Cu₂SnS₃) have diffraction patterns that are close to the one of kesterite CZTS. Absorbance for the same sample is shown in figure 2b. The Tauc plot derived from this measurement is shown in the inset of figure 2b. An estimate of the optical band gap finds a value close to 1.5 eV, in agreement with published values for CZTS^{4, 12, 18}.

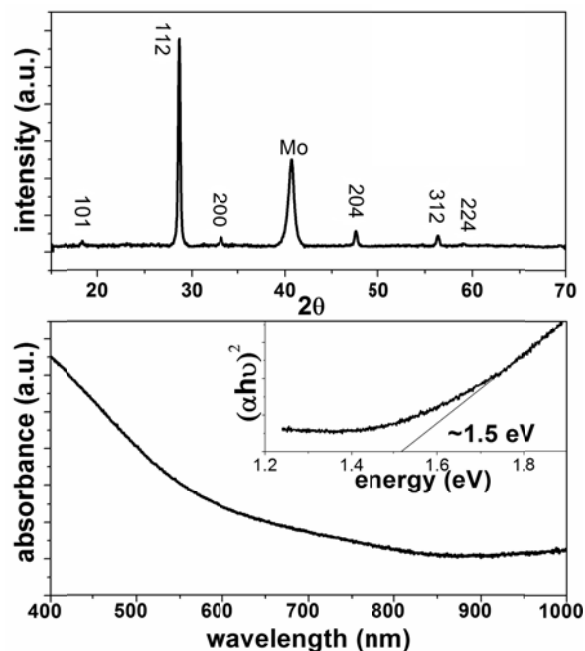


Figure 3. (a) XRD of the sample grown at 460°C. (b) UV-vis absorbance for the sample grown at 460°C. The Tauc plot generated using the absorbance spectrum is shown in the inset.

Elemental analysis has been performed by energy-dispersive X-ray spectroscopy (EDS) in the SEM. The instrument is equipped with an Oxford Instruments Aztec Synergy system. The chemical microanalyses were performed at an accelerating voltage of 5 kV by scanning square areas of 10 μm on the side. Details regarding the EDS quantification and calibration procedures are given in the Supplementary Information. The results, as a function of growth temperature, are shown in table 1. The atomic fractions are averaged from multiple spots and the standard deviation between these readings is used to quantify the uncertainty in the measurement. The film composition strongly depends on growth temperature. We would like to point out that there is large uncertainty in the measurement of the atomic fraction of sulphur, given the fact that some of it is incorporated into the molybdenum substrate (see Raman in figure 1 confirming the presence of MoS₂), and that the thickness of the MoS₂ layer is likely to be temperature-dependent as well. Nevertheless, we find that at low growth temperatures the films are copper rich, while the [Cu]/([Zn]+[Sn]) ratio is near unity at the two highest temperatures. We also find that the films are substantially zinc rich for all the considered growth conditions. We should stress that the elemental analysis has been performed by collecting signal over a large area (~100 micron square), and thus the values reported in table 1 correspond to average and not local compositions.

Table 1: Summary of the results from the elemental analysis performed by EDS on samples grown at different temperatures. The values correspond to atomic percentages and to their ratios.

T(°C)	%Cu	%Zn	%Sn	%S	$\frac{[Cu]}{[Zn]+[Sn]}$	$\frac{[Zn]}{[Sn]}$
360°	38.1(±1.6)	15.5(±0.6)	6.8(±0.5)	39.5(±2)	1.7	2.2

400°	34.8(±0.8)	21.9(±0.5)	8.7(±0.3)	35.4(±1.6)	1.13	2.5
440°	25.7(±0.8)	25(±0.7)	9.5(±0.5)	39.7(±1.9)	0.75	2.6
460°	29.8(±1)	21(±0.6)	10.5(±0.4)	38.7(±1.6)	0.94	2

The issue of thermodynamics stability and phase purity in this material system is well-known¹⁹⁻²¹. We have performed a detailed transmission electron microscopy (TEM) study on the platelets grown at 460°C, and have found evidence of the presence of a copper-rich phase. TEM analysis was performed on a CM300 TEM equipped with EDAX Genesis EDS system. For this analysis, the nano-platelets have been gently removed from the surface with a razor blade and dispersed in methanol. The solution was then drop-cast onto a lacey-carbon-coated nickel TEM grid. Results from this study are summarized in figure 4. The bright field image in figure 4a

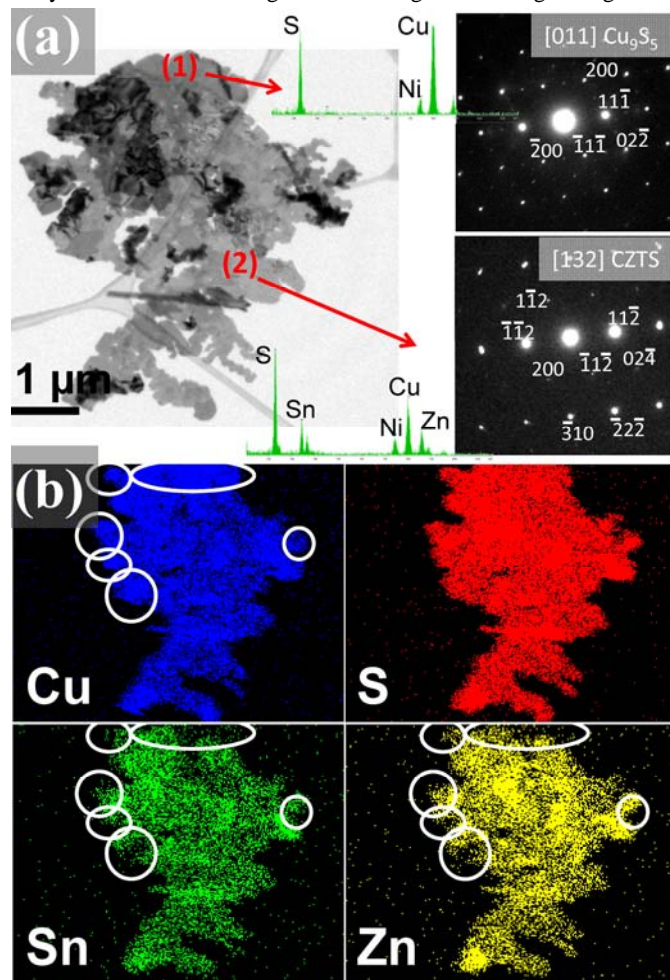


Figure 4. (a) TEM of a nanoplatelet grown at 460°C. EDS scans and selected area diffraction pattern for two spots are also shown. (b) Elemental mapping for the platelet in (a) showing the variation in the local composition.

indicates that the platelet has a complex morphology and structure. The variation in contrast is due mostly to amplitude contrast consequence of difference in crystal orientation as well as variable thickness and composition of the platelets. We have performed elemental analysis and selected area diffraction in two different spots of the platelet. The spots are labelled as (1) and (2) and the corresponding spectra EDS and diffraction data are also shown in figure 4a. The EDS response was calibrated using the appropriate standards. The details of the calibration procedure are given in the Supplementary Information. Spot (1) is copper-rich and its selected

area diffraction pattern can be indexed as [011] zone axis pattern of copper sulphide (Cu_9S_5) with digenite structure²². Weaker reflections, not indexed for the sake of clarity, belong to adjacent crystals that were selected by the diffraction aperture. They can be indexed with CZTS phases²². The EDS spectrum from spot (2) clearly indicates the presence of Zn and Sn as well. The selected area diffraction pattern for spot (2) can be indexed as [132] zone axis of CZTS with kesterite structure²². The weaker reflections indexed as 200, $\bar{1}1\bar{2}$, $02\bar{4}$ and $1\bar{1}2$ actually are from the [021] zone axis, suggesting that more than one grain contributes to the pattern acquired for spot 2. The results from the EDS analysis for spots (1) and (2) are summarized in table 2, in which we also report the composition obtained by selecting the whole platelet shown in figure 4a during the EDS data acquisition. The procedure used to estimate the uncertainty in this measurement is given in the Supplementary Information.

Table 2: Summary of the results from the elemental analysis performed via TEM and shown in figure 4. The value correspond to atomic percentages and to their ratios (last two columns).

Spot	%Cu	%Zn	%Sn	%S	[Cu]	[Zn]
					[Zn]+[Sn]	[Sn]
(1)	56(±3.4)	0.3(±0.3)	1.3(±0.5)	42.5(±3.2)	34	0.2
(2)	25(±1.6)	10.3(±0.8)	18.4(±1.4)	46.3(±3)	0.9	0.56
whole platelet	23.5(±1.4)	10.3(±0.7)	18.6(±1.2)	47.5(±2.8)	0.81	0.55

Consistent with the diffraction analysis, spot (1) is practically free of Zn and Sn, while spot (2) has clear signal from Zn and Sn, with an abundance of Sn with respect of Zn. The composition of the whole platelet is close to the one of spot (2), suggesting that only a minority of the volume is Cu-rich and Zn- and Sn-poor. This conclusion is supported by the elemental mapping, shown in figure 4b. We have circled the areas showing a clear signal from Cu, including the one corresponding to spot (1) in figure 4a, while showing a negligible signal from Sn and Zn. Interestingly, the copper-rich regions are at the edges of the nanoplatelet. Both Raman and XRD data do not show the presence of copper-rich phases, likely because they occupy only a small fraction of the sample volume.

In addition to these data, we would like to report the results of preliminary experiments that suggest that a copper-rich phase is necessary to obtain growth of these two-dimensional nanostructures. We have prepared samples using the same spray pyrolysis technique used for CZTS but selecting only one metal thiocarbamate precursor at the time. Nanostructured films without any sign of anisotropic growth have been obtained when $\text{Sn}[\text{dedc}]_4$ and $\text{Zn}[\text{dedc}]_2$ are used. Anisotropic growth was observed when $\text{Cu}[\text{dedc}]_2$ was used. This observation, in combination with the fact that the copper-rich regions are localized at the edge of the platelets, suggests that copper sulphide might play a catalytic role in the growth of these vertically oriented structures.

There is a significant difference in the composition measured by SEM-EDS for the 460°C sample, which shows a [Zn]/[Sn] ratio of ~2, compared to the elemental analysis performed by TEM, which shows a [Zn]/[Sn] ratio of ~0.5. This is likely the result of the fact that the sample is not homogeneous and that the first of these two measurements is averaged over several platelets, while the second is specific to one particular platelet. Control of the sample composition is not trivial in this system: we have performed experiments in which we have varied the molar ratio between the metal thiocarbamates, and have observed only minor changes in the average film composition, as measured by SEM-EDS. This indicates that the growth proceeds in a kinetically limited regime. A more

sophisticated approach is going to be necessary to precisely control the film composition, which will be the subject of future investigations.

Conclusions

We have demonstrated that nanostructured CZTS films can be grown directly on molybdenum using a standard technique such as spray pyrolysis and using metal diethyldithiocarbamates as precursors. Raman, XRD and optical characterizations confirm the successful growth of CZTS. In-depth TEM characterization confirms the presence of a copper-rich phase which may play a crucial role in the vertical growth of these structures. While the CZTS system is of great interest for thin film photovoltaic devices, these nanostructured films are expected to be relevant for important applications such as for photo-electrochemical devices and for solar-fuel production.

This work was supported primarily by the National Science Foundation under Award Number 1125660. Partial support from the National Science Foundation under Award number 1351386 (CAREER) is also acknowledged. Raman, XRD and optical characterization were performed at the Analytical Chemistry Instrumentation Facility (ACIF) in the Chemistry Department at UC Riverside. TEM characterization was performed at the Central Facility for Advanced Microscopy and Microanalysis (CFAMM) at UC Riverside.

Notes and references

^a Mechanical Engineering Department, University of California Riverside, 900 University Avenue, Riverside CA 92521.

^b Central Facility for Advanced Microscopy and Microanalysis, University of California Riverside, 900 University Avenue, Riverside CA 92521.

^c Materials Science and Engineering Program, University of California Riverside, 900 University Avenue, Riverside CA 92521.

Electronic Supplementary Information (ESI) available: [details of any supplementary information available should be included here]. See DOI: 10.1039/c000000x/

1. Q. J. Guo, H. W. Hillhouse and R. Agrawal, *J. Am. Chem. Soc.*, 2009, **131**, 11672-+.
2. T. K. Todorov, K. B. Reuter and D. B. Mitzi, *Adv. Mater.*, 2010, **22**, E156-E159.
3. Q. Guo, G. M. Ford, W. C. Yang, B. C. Walker, E. A. Stach, H. W. Hillhouse and R. Agrawal, *J. Am. Chem. Soc.*, 2010, **132**, 17384-17386.
4. D. B. Mitzi, O. Gunawan, T. K. Todorov, K. Wang and S. Guha, *Sol. Energy Mater. Sol. Cells*, 2011, **95**, 1421-1436.
5. W. Wang, M. T. Winkler, O. Gunawan, T. Gokmen, T. K. Todorov, Y. Zhu and D. B. Mitzi, *Advanced Energy Materials*, 2014, **4**, n/a-n/a.
6. W. Shockley and H. J. Queisser, *J. Appl. Phys.*, 1961, **32**, 510-519.
7. N. Kamoun, H. Bouzouita and B. Rezig, *Thin Solid Films*, 2007, **515**, 5949-5952.
8. H. Yoo and J. Kim, *Sol. Energy Mater. Sol. Cells*, 2011, **95**, 239-244.
9. V. G. Rajeshmon, C. S. Kartha, K. P. Vijayakumar, C. Sanjeeviraja, T. Abe and Y. Kashiwaba, *Solar Energy*, 2011, **85**, 249-255.
10. Y. B. Kishore Kumar, G. Suresh Babu, P. Uday Bhaskar and V. Sundara Raja, *Sol. Energy Mater. Sol. Cells*, 2009, **93**, 1230-1237.

11. D. Pan, L. An, Z. Sun, W. Hou, Y. Yang, Z. Yang and Y. Lu, *J. Am. Chem. Soc.*, 2008, **130**, 5620-5621.
12. A. Khare, A. W. Wills, L. M. Ammerman, D. J. Norris and E. S. Aydil, *Chem. Commun.*, 2011, **47**.
13. S. Liu, H. W. Zhang and M. T. Swihart, *Nanotechnology*, 2009, **20**.
14. P. Davis and L. Mangolini, *MRS Communications*, 2013, **3**, 57-60.
15. A.-J. Cheng, M. Manno, A. Khare, C. Leighton, S. A. Campbell and E. S. Aydil, *Journal of Vacuum Science & Technology A*, 2011, **29**, 051203.
16. P. A. Fernandes, P. M. P. Salome and A. F. da Cunha, *Journal of Alloys and Compounds*, 2011, **509**, 7600-7606.
17. H. Li, Q. Zhang, C. C. R. Yap, B. K. Tay, T. H. T. Edwin, A. Olivier and D. Baillargeat, *Advanced Functional Materials*, 2012, **22**, 1385-1390.
18. K. Tanaka, N. Moritake and H. Uchiki, *Sol. Energy Mater. Sol. Cells*, 2007, **91**, 1199-1201.
19. A. Polizzotti, I. L. Repins, R. Noufi, S. H. Wei and D. B. Mitzi, *Energy & Environmental Science*, 2013, **6**, 3171-3182.
20. N. J. Carter, W. C. Yang, C. K. Miskin, C. J. Hages, E. A. Stach and R. Agrawal, *Sol. Energy Mater. Sol. Cells*, 2014, **123**, 189-196.
21. J. J. Scragg, T. Ericson, T. Kubart, M. Edoff and C. Platzer-Bjorkman, *Chem. Mat.*, 2011, **23**, 4625-4633.
22. V. Dimov, V. Iamakov and K. Bozhilov, *Computers & Geosciences*, 1994, **20**, 1267-1273.